ELSEVIER

Biochimica et Biophysica Acta 1229 (1995) 215–224

BBA Biochimica et Biophysica Acta

Vibrational coherence and relaxation dynamics in the primary donor state of the mutant reaction center of *Rhodobacter capsulatus*: Theoretical analysis of pump-probe stimulated emission

X.Z. Gu [a], M. Hayashi [a,b,*], S. Suzuki [a], S.H. Lin [a,b]

[a] *Department of Chemistry and Biochemistry, The Center for the Study of Early Events in Photosynthesis, Arizona State University, Box 871604, Tempe, AZ 85287-1604, USA*

[b] *Institute of Atomic and Molecular Sciences, Academia Sinica, P.O. Box 23-166 Taipei, Taiwan 107, Republic of China*

Received 2 December 1994; accepted 7 December 1994

Abstract

The effects of vibrational coherence and vibrational relaxation on the pump-probe stimulated emission are theoretically studied on the basis of the perturbative density operator method and the transient linear susceptibility theory. The time-resolved profiles are simulated for the system with the single vibrational mode at the several temperature at the several probing frequencies. The quantum beats appeared in the profiles are shown to rapidly dephase as the temperature increases. The calculations imply that the time constant of the vibrational relaxation of the intra-dimer mode in the special pair of the D_{LL} mutant of *Rhodobacter capsulatus* is approximately the order of 300 femtosecond at the low temperatures.

Keywords: Photosynthetic reaction center; Electron transfer; Vibrational relaxation; Vibrational coherence; Ultrafast spectroscopy (R.capsulatus)

1. Introduction

Recently, femtosecond chemistry has considerably attracted experimental and theoretical attention. The application of femtosecond measurements to biological systems reveals ultra-fast phenomena [1–3], such as quantum beats and their decays that, respectively, represent the coherent motions and the relaxation of vibrational modes [2,3]. In particular, the initial electron transfer (ET) in photosynthetic reaction centers (RCs) is most appealing, since ultra-fast components associated with the ET are found in the time-resolved profiles. By applying femtosecond spectroscopy and/or mutagenetic techniques toward the elucidation of the ET mechanism, the intensive work on the ultra-fast ET in RCs has been reported [4–28]. In this paper, we report a theoretical treatment of the vibrational coherence and its relaxation that takes place in photosynthetic RCs at low temperatures.

The bacterial photosynthetic RC has been characterized in greater details, both structurally and functionally, than any another integral membrane protein complex [29–31]. One of the characteristics of the structure of the RC is its pseudo-C_2 symmetry that extends to the level of the cofactors forming two branches (L and M). In addition, the ET is only active in one of the branches (L). The special pair P, a pair of bacteriochlorophyll (*BChl*) molecules, is situated in the pseudo-C_2 symmetry axis and near the periplasmic side of the membrane. It is generally agreed that in photosynthetic ET, excitation of the P to P^* initiates the first ET process, in which the electronically excited state P^* lives with a time constant of next 1–4 ps, leading to the charge separated state $P^+H_L^-$, a reduced bacteriopheophytin (*BPhe*) H_L^-, on the M branch. Electron transfer from H_L^- to Q_L a primary quinone on the L branch, proceeds with a time constant of about 200 ps and is followed by subsequent transfer from Q_L to another primary quinone Q_M on the M branch in hundreds of microseconds, which completes the ET. Since the back reaction times are all at least an order of magnitude slower than the forward one, the quantum yield is near unity.

A related and much investigated question concerns the mechanism of ET between P and H_L, and to what extent the state $P^+B_L^-$ is actually populated or involved as a

* Corresponding author. Fax: +1 602 9652747.

SSDI 0005-2728(94)00197-9

virtual state allowing direct ET [9–20,32–39]. Since higher-resolution transient absorption experiments were performed [11,13], it was discovered that one could not model the initial ET reaction as a single-exponential decay of $P^+H_L^-$ at all wavelengths. It became clear that the room-temperature decay kinetics were dependent on wavelength.

Kirmaier and Holten [11], have proposed that the wavelength dependence results from conformational heterogeneity in the RC population (one-step model). In addition, employing bleaching kinetics of H_L based on the sequential two-step mechanism, Fleming's group have also observed that decays of P^* can not be fitted to a single exponential function [6]. Recent work from the same laboratory has suggested a combination of sequential and superexchange models to interpret the spontaneous emission of P^* [16].

Quite recently, Zinth and his co-worker have reported the sub-picosecond kinetic component in transient absorption spectra of RCs of *Rhodobacter (Rb.) sphaeroides* and *Rhodopseudomonas (Rps.) viridis*, suggesting a third kinetic process characterized by an extremely short time constant of 0.9 ps and 0.65 for *Rb. sphaeroides* and *Rps. viridis*, respectively [13,17]. They have analyzed those measurements of the wavelength-dependent kinetics in terms of a spectral analysis of the decay component amplitudes and argue for a model involving $P^+B_L^-$ or the formation of a short-lived *Bchl* anion, B_L^- (two-step model), which had been proposed by Shuvalov and co-workers [35]. Although their data showed no quantum beats, one should investigate the possibility of non-equilibrated vibrational motions in the $P^+B_L^-$ and the effects of such vibrational motions on the ET from the microscopic point of view. The experimental studies conducted thus far have led to the qualitative observation that the interpretation of the kinetics at a single or a few selected wavelengths is problematic. The amplitudes of a kinetic analysis, for instance, are not directly representative of the populations in intermediate states (if they exist) but, rather, are complicated by the extinction coefficients of the participating states and the proposed mechanism itself.

Recently, reporting short-lived oscillations in the time-resolved profile at a temperature of 10 K, Vos et al. have performed femtosecond pump-probe stimulated emission measurements on D_{LL} mutant RCs of *Rb. capsulatus* and *R26* mutant RCs of *Rb. sphaeroides* [1]. Lacking of the H_L, the D_{LL} mutant undergoes no ET during the femtosecond measurements. In our previous paper [39], proposing the vibrational relaxation time of 500 fs, we analyzed their data based on the perturbative density matrix and susceptibility methods. This vibrational mode is associated with intra-dimer vibrations in the special pair [41]. Quite recently, the same laboratory has reported more detailed femtosecond experimental data on D_{LL} mutant RCs of *Rb. capsulatus*, providing the effects of temperature, excitation and probing wavelength on the pump-probe stimulated emission [2]. The time-resolved profiles show a distinctive slow oscillatory component in addition to the fast oscillatory ones that is presumably related to intra-dimer vibrations in the special pair. The Fourier analysis of the quantum beats implies that the frequency of the slow oscillatory component is approximately 17 cm^{-1}, which is associated presumably with vibrational motions of proteins in the membrane of the D_{LL} mutant RC. Small and his co-workers have emphasized the importance of protein modes in absorption spectra of RCs as well [42,43]. The quantum beats appearing in the time-resolved profiles strongly indicate that the vibrational relaxation takes place during the femtosecond measurements at low temperatures; situation that the conventional ET theory is not applicable.

The complexities of the ET in the RCs at low temperatures are not only due to the non-equilibrated vibrational motions but also because of inhomogeneities in the structural conformations of the RCs. Boxer and his co-workers [44] and Small and his co-workers [45,46] have performed hole-burning measurements on wild-type RCs and mutant RCs: both of them reporting a number of constants of homogeneous broadening in the electronic transition frequencies and a various number of high (small) vibrational frequencies and their coupling constants that are assigned to the intra-dimer (protein) modes. However, it has not been resolved to what extent vibrational relaxation and inhomogeneities affect the ET dynamics at low temperatures and the ultra-short time-resolved profiles of transient spectroscopy.

The conventional ET theory is a powerful tool to investigate the mechanisms of ET taking place in the systems in which a weak electronic coupling, a single vibrational mode with a strong coupling constant, and the vibrational equilibrium are assumed [47–51]. Thus, this theory is not applicable to the ultra-short time regions over which ET takes place accompanying vibrational relaxation or to the systems consisting of a multi-mode with weak coupling constants. In such ultra-short time regions, one should analyze the ET dynamics on the basis of single-vibronic level ET rate constants taking into account the vibrational relaxation as well. In addition, it became clear that the photosynthetic ET involved several vibrational modes. Using semi-empirical molecular orbital calculations, Warshel determined six vibrational modes; four high-frequency modes with small coupling constants and two low-frequency ones, one of whose coupling constant is rather large. The high-frequency modes, with small coupling constants, do not play an important role in absorption or emission spectra. However, in a previous paper, we have shown that these high-frequency modes play an important role in ET, especially for the case in which the electronic energy gap is larger than 200 cm^{-1}. These modes have also been observed in resonance Raman scattering [52,53]. As already mentioned above, applying hole-burning techniques, Small's group measured small-frequency modes; a

frequency of 120 and 145 cm^{-1} *Rb. sphaeroides* RCs and *Rps. viridis* RCs, respectively [45]. Analyzing the experimental data, they found that the coupling constants of these modes are quite large compared with the high-frequency modes. In addition, observing a mean phonon frequency of 30 cm^{-1} and a one-phonon profile width of approximately 40 cm^{-1}, they have reported phonon-side-bands in the hole burning spectra [45]. From their detailed analysis of the hole-burning experimental data, they found that the RCs of *Rb. sphaeroides* and *Rps. viridis* undergo sub-pico second relaxation processes [45]. Thus, the single-vibronic level ET rate constants should incorporate the multi-mode in the RCs [54].

In our previous work [55,56], we have analyzed the femtosecond time-resolved three-dimensional spectra of *Rb. sphaeroides* at room temperature by applying an excitonic-vibronic coupling model in which, including the excitonic states of the dimer P, 10 electronic states were used. Our analysis strongly indicated that more than three electronic states are required in order to construct the observed, femtosecond time-resolved spectra and interpret the wavelength-dependent kinetics and that the multi-mode effect should be considered in calculation of the ET rate.

Detailed analyses would be a great task indeed, ranging the frequency domain experiments to the time-resolved measurements. It is most important, however, to utilize those experimental data for establishing a whole scheme of the ET mechanism of RCs at various temperatures. In this work, focusing on the vibrational relaxation and its temperature dependence, we present theoretical analysis of the quantum beats appeared in pump-probe stimulated emission profiles on the D_{LL} mutant RCs of *Rb. capsulatus* [2]. Since this system show no ET during femtosecond measurements as mentioned above, we can isolate vibrational relaxation information, which leads to more precise and detailed mutual analyses of the hole-burning spectra and absorption spectra at low temperatures.

In the following section, we briefly describe out theoretical treatment. On the basis of the perturbative density operator method [57,58] and the transient linear susceptibility theory [59–61], we can properly incorporate both pumping and probing optical processes as well as vibrational dynamics taking place between them. In discussion, we shall show the effects of temperature on pumping-probe stimulated emission spectra, and on how quantum beats are modulated as a result.

2. Theoretical

We consider a model for the pump-probe stimulated emission measurement in which a pumping laser pulse excites molecules in a ground vibronic manifold $\{g\}$ to an excited vibronic manifold $\{n\}$ and a probing pulse applied to the system after the excitation. The probing laser induces stimulated emission in which transitions from the manifold $\{n\}$ to the ground state manifold $\{m\}$ take place. We assume that there is no overlap between the two optical processes and they are separated by a time interval τ. On the basis of the perturbative density operator method, we can derived an expression for the time-resolved profiles which are associated with the imaginary part of the transient linear susceptibility [58–60], i.e.,

$$\overleftrightarrow{\chi}''(\omega_{pr},\tau) = -\frac{1}{\hbar}\sum_{n,n'}\sum_{m}\mathrm{Im}\left\{\rho_{n,n'}(\tau)\frac{i(\vec{\mu}_{n',m}\otimes\vec{\mu}_{m,n})}{i(\omega_{n',m}-\omega_{pr})+1/T_{pr}}\right\} \quad (1)$$

where $\rho_{n,n'}(\tau)$ denotes the density matrix element, ω_{pr}, $1/T_{pr}$, $\omega_{n',m}$ and $\vec{\mu}_{n',m}$ are, respectively, the central frequency of the probing laser pulse, its bandwidth, the transition frequency and the transition dipole moment.

Based on Eq. (1), we shall derive a single-mode representation of $\overleftrightarrow{\chi}(\omega_{pr},\tau)$. In the adiabatic approximation, one can find $|n\rangle = |b\rangle|bv\rangle$, $|n'\rangle = |b\rangle|bv'\rangle$, $|m\rangle = |a\rangle|au\rangle$ and $|m'\rangle = |a\rangle|au'\rangle$ where b and a, respectively, represent the electronically excited and ground states and v or v' (u or u') is the vibrational state in the electronic state b (a). We assume that the probing pulse is such short that molecular dephasing processes during the optical process can be ignored. Using the above basis set, Eq. (1) becomes

$$\overleftrightarrow{\chi}''(\omega_{pr},\tau) = -\frac{1}{\hbar}\sum_{v,v'}\sum_{u}\mathrm{Im}\left\{\rho_{bv,bv'}(\tau)\frac{i(\vec{\mu}_{bv',au}\otimes\vec{\mu}_{au,bv})}{i(\omega_{bv',au}-\omega_{pr})+1/T_{pr}}\right\} \quad (2)$$

One can easily find in Eq. (2) that $\overleftrightarrow{\chi}''(\omega_{pr},\tau)$ consists of the coherent part $\chi''_{co}(\omega_{pr},\tau)$ and the incoherent part $\chi''_{in}(\omega_{pr},\tau)$, i.e.,

$$\chi''(\omega_{pr},\tau) = \chi''_{in}(\omega_{pr},\tau) + \chi''_{co}(\omega_{pr},\tau), \quad (3)$$

where

$$\overleftrightarrow{\chi}''_{in}(\omega_{pr},\tau) = -\frac{1}{\hbar}\sum_{v}\sum_{u}\mathrm{Im}\left\{\rho_{bv,bv}(\tau)\frac{i(\vec{\mu}_{bv,au}\otimes\vec{\mu}_{au,bv})}{i(\omega_{bv,au}-\omega_{pr})+1/T_{pr}}\right\} \quad (4)$$

and

$$\overleftrightarrow{\chi}''_{co}(\omega_{pr},\tau) = -\frac{1}{\hbar}\sum_{v\neq v'}\sum_{u}\mathrm{Im}\left\{\rho_{bv,bv'}(\tau)\times\frac{i(\vec{\mu}_{bv',au}\otimes\vec{\mu}_{au,bv})}{i(\omega_{bv',au}-\omega_{pr})+1/T_{pr}}\right\} \quad (5)$$

where $\omega_{bv',au} = \omega_{b,a} + (v' - u)\omega$ and $\omega_{b,a}$ is the electronic transition frequency and ω denotes the vibrational frequency. The first and second terms on the right hand side of Eq. (3) are associated with the dynamics of vibrational population and coherence. We shall first consider the population dynamics. In the Condon approximation, Eq. (4) becomes

$$\overleftrightarrow{\chi}''_{in}(\omega_{pr},\tau) = -\frac{(\vec{\mu}_{b,a} \otimes \vec{\mu}_{a,b})}{\hbar} \times \sum_{v} \mathrm{Re}\{\rho_{bv,bv}(\tau) F_{bv,bv}(\omega_{pr})\} \quad (6)$$

Here $F_{bv,bv}(\omega_{pr})$ denotes the bond-shape function of $\overleftrightarrow{\chi}_{in}(\omega_{pr},\tau)$ and is given by

$$F_{bv,bv}(\omega_{pr}) = \sum_{u} \frac{|\langle au|bv\rangle|^2}{i(\omega_{bv,au} - \omega_{pr}) + 1/T_{pr}}, \quad (7)$$

where $\langle au|bv\rangle$ denotes the overlap integral of the vibrational wave functions. The vibrational overlap is expressed, in terms of the displaced harmonic oscillator basis, as

$$\langle au|bv\rangle = e^{-S/2} \sum_{i=0}^{v} \sum_{j=0}^{u} \delta_{u-j,v-i} S^{(i+j)/2} \times \frac{v!}{i!(v-i)!} \left(\frac{u!}{v!}\right)^{1/2} \frac{(-1)^j}{j!} \quad (8)$$

where S is the coupling constant (or Huang-Rhys factor) associated with the displacement in the normal coordinate between the equilibrium positions of each potential. Hereafter we ignore the suffix b in $\rho_{bv,bv}(\tau)$ for simplicity. The temporal development of the population in the vibrational state v, $\rho_{v,v}(\tau)$, satisfies the master equation [62];

$$\frac{\partial \rho_{v,v}(\tau)}{\partial \tau} = -\Gamma^{v,v}_{v,v}\rho_{v,v}(\tau) + \sum_{\substack{v' \neq v \\ \text{and/or} \\ v'' \neq v}} \Gamma^{v',v''}_{v,v}\rho_{v',v''}(\tau) \quad (9)$$

where $\Gamma^{v,v}_{v,v}$ denotes the population decay constant of the vibrational state v and the diagonal element of $\Gamma^{v',v''}_{v,v}$, for example, $\Gamma^{v',v'}_{v,v}$ represents the rate constant of the vibrational population transfer from v' to v, while the off-diagonal element, i.e., $v \neq v'$, stands for the vibrational coherence transfer from $v \leftrightarrow v'$ to $v \leftrightarrow v$. Those decay and transfer processes are induced by an interaction with the heat-bath modes. Having focused on the vibrational relaxation, we have ignored in the derivation of Eq. (9) the vibrational couplings that deplete the electronically excited state via non-radiative transitions.

In the secular approximation [57,58], we can eliminate the coherence terms, for instance $\rho_{v',v''}(\tau)$ $(v' \neq v'')$, in Eq. (9) such that the only diagonal terms contribute to the vibrational transitions through which the vibrational populations in various states are coupled. By applying the ladder model [62] to the interaction between the vibrational and heat-bath modes, the vibrational population decay constant $\Gamma^{v,v}_{v,v}$ is expressed as

$$\Gamma^{v,v}_{v,v} = \{v + (1+v)\exp(-\hbar\omega/k_BT)\}\gamma_{1\to 0}. \quad (10)$$

The first term in Eq. (10) is originated from the decay from v to $v-1$, while the second one, with the Boltzmann factor, is due to the thermally activated transition from v to $v+1$. The vibrational population transfer, on the other hand, is only allowed to undergo the $v \to v \pm 1$ transitions in the ladder model. Thus, the rate constant of the transfer is given by

$$\Gamma^{v',v''}_{v,v} = \Gamma^{v-1,v-1}_{v,v}\delta_{v',v-1}\delta_{v'',v-1} + \Gamma^{v+1,v+1}_{v,v}\delta_{v',v+1}\delta_{v'',v+1} \quad (11)$$

where $\Gamma^{v-1,v-1}_{v,v}$ and $\Gamma^{v+1,v+1}_{v,v}$ pertain to, respectively, the vibrational population transfer from v to $v+1$ and that from $v+1$ to v, and they are given by

$$\Gamma^{v-1,v-1}_{v,v} = v\exp(-\hbar\omega/k_BT)\gamma_{1\to 0} \quad (12)$$

and

$$\Gamma^{v+1,v+1}_{v,v} = (1+v)\gamma_{1\to 0}. \quad (13)$$

One can easily see from Eq. (12) that the population transfer from $v-1$ to the above state takes place via accepting energy from the heat bath-modes. Notice that $\gamma_{1\to 0}$ in Eq. (11) represents the rate constant of the vibrational transition $v = 1 \to v = 0$ and is given by [62]

$$\gamma_{1\to 0} = \frac{2\pi}{\hbar}\frac{1}{2C^2}\sum_{\alpha,\beta} P_\alpha |\langle \beta|\hat{F}_B|\alpha\rangle|^2 \delta(E_\beta - E_\alpha - \hbar\omega) \quad (14)$$

where $C^2 = \omega/\hbar$, and α and β (E_α and E_β) denote the states of the heat bath-modes (their energies), $\hat{F}_B$ is the heat bath operator, P_α represents the thermal distribution function if the heat bath-modes. Substituting Eqs. (10–11) into Eq. (9), one can obtain

$$\frac{\partial \rho_{v,v}(\tau)}{\partial \tau} = -\{v + (1+v)\exp(-\hbar\omega/k_BT)\}\gamma_{1\to 0}\rho_{v,v}(\tau) + (1+v)\gamma_{1\to 0}\rho_{v+1,v+1}(\tau) + v\exp(-\hbar\omega/k_BT)\gamma_{1\to 0}\rho_{v-1,v-1}(\tau), \quad (15)$$

where the terms with the Boltzmann factor are associated with the thermally induced vibrational transitions as mentioned above; they vanish at low temperature, when $\hbar\omega \gg k_BT$ holds.

With the ultra-short pulse excitation, the initial condition of Eq. (15) is given by [58–60]

$$\rho_{v,v}(0) = \left|\frac{\vec{\mu}_{b,a}\cdot\vec{E}_{pu}(\omega_{pu})}{\hbar}\right|^2 \sum_{u'} P_{u'}|\langle bv|au'\rangle|^2, \quad (16)$$

where $P_{u'} = \exp(-u'\hbar\omega/k_BT)/\{1 - \exp(-\hbar\omega/k_BT)\}$. The initial condition is a function of S as seen in Eq. (8).

The coherent component, i.e., Eq. (5) can be treated in a similar fashion as well and one can find

$$\overleftrightarrow{\chi}''_{CO}(\omega_{pr},\tau) = -\frac{(\vec{\mu}_{b,a}\otimes\vec{\mu}_{a,b})}{\hbar}\sum_{v,v'}^{v\neq v'}\mathrm{Re}\{\rho_{bv,bv'}(\tau)F_{bv,bv'}(\omega_{pr})\}, \quad (17)$$

where

$$F_{bv,bv'}(\omega_{pr}) = \sum_u \frac{\langle bv'|au\rangle\langle au|bv\rangle}{i(\omega_{bv',au}-\omega_{pr})+1/T_{pr}}. \quad (18)$$

in the secular approximation and with the ladder model, the time evolution of the vibrational coherence, $\rho_{v,v'}(\tau)$, is determined by

$$P_{v,v'}(\tau) = \exp\{-(i\omega_{v,v'} + \Gamma_{v,v'}^{v,v'})\tau\}\rho_{v,v'}(0), \quad (19)$$

where $\omega_{v,v'} = (v - v')\omega$ and

$$\rho_{v,v}(0) = \left|\frac{\vec{\mu}_{b,a}\cdot\vec{E}_{pu}(\omega_{pu})}{\hbar}\right|^2 \sum_{u'} P_{u'}\langle bv'|au'\rangle\langle au'|bv\rangle. \quad (20)$$

By omitting the pure dephasing processes, which is warranted at low temperatures, the dephasing constant $\Gamma_{v,v'}^{v,v'}$ in Eq. (19) can be expressed, in terms of the population decay constants of the states v and v', as

$$\Gamma_{v,v'}^{v,v'} = \tfrac{1}{2}\{v + v' + (2 + v + v')\exp(-\hbar\omega/k_BT)\}\gamma_{1\to 0}. \quad (21)$$

Having considered only the single mode case so far, we can also derive an expression of $\overleftrightarrow{\chi}''(\omega_{pr},\tau)$ for a multimode system in a similar fashion. In two mode case, for instance, $\overleftrightarrow{\chi}''(\omega_{pr},\tau)$ can be divided into three terms, each of which corresponds to interference between the vibrational processes of the two modes. It should be noted here that within the same approximations as used above, the density matrix of the two modes during the time interval τ can be expressed as a product of each mode's matrix.

3. Result and discussion

In order to investigate how vibrational relaxation affects ultra-fast dynamics that appear in the profiles of pump-probe stimulated emission, we now utilize the equations derived in section 2 and apply them to analysis of the time-resolved profiles of D_{LL} mutant RCs of *Rb. capsulatus* reported by Vos et al. [2]. In order to determine reasonable molecular parameters for vibrational frequencies and the coupling constants, we analyzed absorption spectra of D_{LL} mutant RCs. Since hole-burning spectra of D_{LL} mutant RCs of *Rb. capsulatus* have not been reported so far, there is ambiguity to determine how many vibrational modes, especially small-frequency modes related to the protein motions or the intra-dimer vibrations, are exhibited by the absorption and stimulated emission spectra. Thus, taking into account analyses of hole-burning spectra of RCs of *Rb. sphaeroides* reported by Small's group [45] and based on our previous work [40], we shall focus on the case in which a system consists of a single mode; we set the coupling constant $S = 2.5$, the vibrational frequency $\omega = 100\ \mathrm{cm}^{-1}$ and the vibrational transition rate constant $\gamma_{1\to 0} = 3\ \mathrm{ps}^{-1}$. It should be noted that $S\omega = 250\ \mathrm{cm}^{-1}$ is basically identical to that determined by Small's group [45].

At an extremely low temperature, e.g., $\hbar\omega \gg k_BT$, Eq. (15) becomes

$$\frac{\partial\rho_{v,v}(\tau)}{\partial\tau} = -v\gamma_{1\to 0}\rho_{v,v}(\tau) + (1+v)\gamma_{1\to 0}\rho_{v+1,v+1}(\tau) \quad (22)$$

where no thermally activated processes take place. According to the ladder model, the rate constant of vibrational transition $v + 1 \to v$ is proportional to the quantum number of $v + 1$. Assuming the system is excited as at such a low temperature, we first solve this coupled equation numerically. In this case, the initial condition is given by

$$\rho_{v,v}(0) \approx |\langle bv|a0\rangle|^2 = S^v\frac{e^{-S}}{v!}. \quad (23)$$

On can easily see from Eq. (23) that all the transitions start from $u = 0$ and the most probable transition occurs at $v = 2$. Fig. 1 shows temporal development of the populations in the vibrational states $v = 0$, 1, 2 and 3 of the

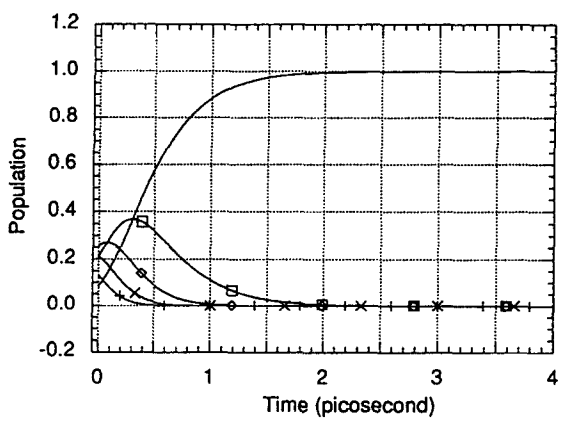

Fig. 1. Temporal development of the vibrational populations of the model system at 10 K. The pure solid line, the ones with □, ◇, × and + represent, respectively, the populations in the vibrational states $v = 0$, 1, 2, 3 and 4. The calculation utilizes Eq. (22). The parameters are the coupling constant $S = 2.5$, the vibrational frequency $\omega = 100\ \mathrm{cm}^{-1}$ and the vibrational transition rate constant $\gamma_{1\to 0} = 3\ \mathrm{ps}^{-1}$. All the populations are eventually transferred to the state $v = 0$ through the vibrational population transitions after 2.5 ps no populations can be seen in the other states.

system at a temperature 10 K. At this temperature, the Boltzmann factor in Eq. (15) is the order of 10^{-7}, thus, the application of Eq. (22) is warranted. We have solved Eq. (22) self-consistently in order to truncate v, which procedure leads to the coupled equation:

$$\frac{\partial \rho_{v_m,v_m}(\tau)}{\partial \tau} = -v_m \gamma_{1\to 0}\, \rho_{v_m,v_m}(\tau)$$

$$\frac{\partial \rho_{v_m-1,v_m-1}(\tau)}{\partial \tau} = -(v_m-1)\gamma_{1\to 0}\, \rho_{v_m-1,v_m-1}(\tau) + v_m \gamma_{1\to 0}\, \rho_{v_m,v_m}(\tau)$$

$$\frac{\partial \rho_{0,0}(\tau)}{\partial \tau} = \gamma_{1\to 0}\, \rho_{1,1}(\tau), \qquad (24)$$

where v_m represents the maximum quantum number of the vibrational state used in the calculation, and is 15 at 10 K. In Fig. 1, the pure solid line, the ones with □, ◇, × and + stand for, respectively, the populations in the states v = 0, 1, 2, 3 and 4. The only transitions from $u = 0$ to those states make a significant contribution to the vibrational population dynamics. Fig. 1 clearly shows all the populations are eventually accumulated to the state $v = 0$ through the vibrational population transfer, thus, after 2.5 ps no populations can been seen in the other states.

Fig. 2 shows simulation of pump-probe stimulated emission profiles at various probing frequencies at 10 K. In Fig. 2a, the pure solid line and the one with ○ denote the time-resolved profile at 915 nm (10929 cm^{-1}) and 900 nm (11111 cm^{-1}), respectively. In Fig. 2b, the pure solid line, the ones with ○ and × represent the profiles at 960 nm (10417 cm^{-1}) and 930 nm (10753 cm^{-1}), respectively. In addition to the same parameters as used in Fig. 1, we have set the electronic transition frequency $\omega_{ba} = 900$ nm. Fig. 2 clearly shows that the coherent excitation of the vibrational states results in quantum beat in the time-resolved profile at each probing frequency, whose beat oscillation ultimately decreases in amplitude due to the dephasing process through the vibrational population transfer. The profiles at 910 and 930 nm indicate that the peak position of the stimulated emission is located between those two frequencies. It should be noted that the peak position of the stimulated emission is approximately given by $\omega_{ba} - S\omega \approx 920$ nm (10886 cm^{-1}), which is consistent with the spectral data [2]. Figs. 1 and 2 imply that the profiles of the pump-probe stimulated emission at the extremely low temperature mainly reflect the dynamics in the states $v = 0$ and 1.

We now increase the temperature of the system to show how the thermal equilibrium is achieved. For this purpose, taking into account the thermally induced vibrational transitions, i.e. Eq. (15), we solve the coupled equation numerically. Fig. 3a demonstrates time development of the populations in the $v = 0$, 1, 2, 3 and 4 states at a temperature of 50 K. The calculation have utilized the same parameters as used in Fig. 1. Resulting in a turn-over feature in the

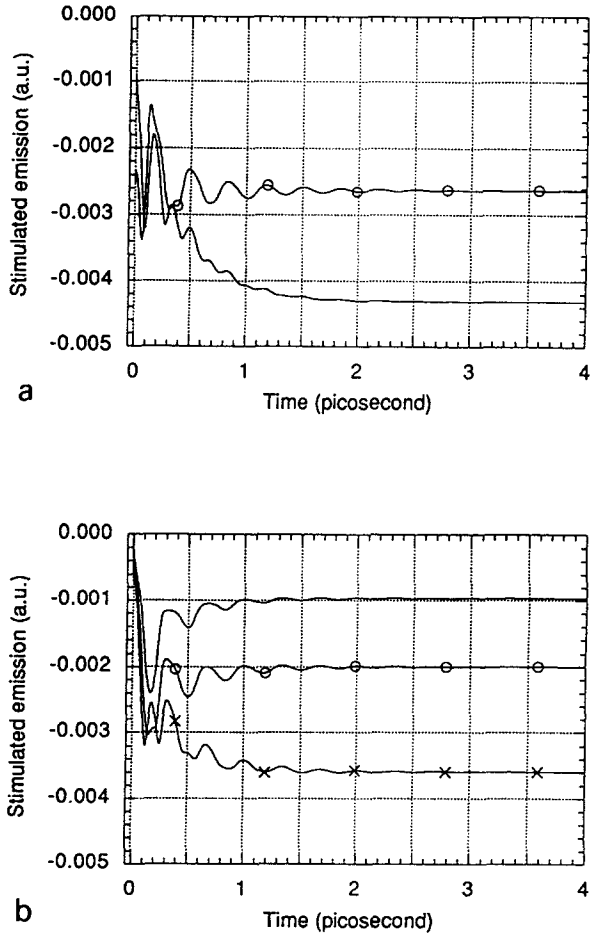

Fig. 2. Simulation of pump-probe stimulated emission profiles at various probing frequencies at 10 K. (a) The pure solid line and the one with ○ represent the time-resolved profile at 915 nm (10929 cm^{-1}) and 900 nm (11111 cm^{-1}), respectively: (b) the pure solid line, the ones with ○ and × depict the profiles at 960 nm (10417 cm^{-1}) and 930 nm (10753 cm^{-1}), respectively. The electronic transition frequency $\omega_{ba} = 900$ nm are used for the calculations. The quantum beat at each probing frequency whose oscillation ultimately decreases in amplitude due to the dephasing process through the vibrational population transfer. The profiles at 910 and 930 nm indicate that the peak position of the stimulated emission is located between those two frequencies.

time-development of the population in the state $v = 1$ within the first 0.5 ps time region, the populations in the states $v = 2$ and 3 rapidly decay within 2 ps. After 2.5 ps all the changes in time-development behavior of each state become a plateau and approach to the thermal equilibrated populations; $n_1/n_0 = 4.62 \cdot 10^{-2}$, $n_2/n_0 = 2.13 \cdot 10^{-3}$, $n_3/n_0 = 9.80 \cdot 10^{-5}$, $n_4/n_0 = 4.52 \cdot 10^{-6}$ (n_i being the population of the state i), which situation indicates that the thermal equilibration is achieved on a time-scale 2.5 ps. At this temperature, we can clearly see large populations in the states $v = 1$ as well as $v = 0$, compared with the case of 10 K. The effect of thermal equilibration is more pronounced in Figs. 3b and 3c at temperatures of 100 and 150 K, respectively. Fig. 3 shows that all the states at each temperature are thermally populated after 2.5 ps and the

populations in all the states up to $v = 3$ are clearly seen after the thermal equilibration is achieved.

Figs. 4, 5 and 6 show simulations of time-resolved profiles of pump-probe stimulated emission at 50, 100 and 150 K, respectively. The calculations have adopted the same parameters as used in Fig. 2. Figs. 5 and 6 show rapid decreases in amplitude within the first 2.0 ps time region. This is mainly due to the fact that the dephasing rate increases through the thermally activated vibrational transitions that are associated with the term with the Boltzmann factor in Eq. (21). Most part of the oscillatory features are found in the first 1.0 ps time region over which the system still maintains the information of the coherent excitation. After 2 ps, the time profiles at 900, 915 and 930 nm, which are near the peak frequency of the stimulated emission spectrum, decrease in intensity as the temperature increases. This implies that at those probing frequencies the profiles reflect the population in the state $v = 0$. At the other frequencies, on the other hand, the profiles gain intensity as the temperature increases, which results from the thermal equilibration of the vibrational states.

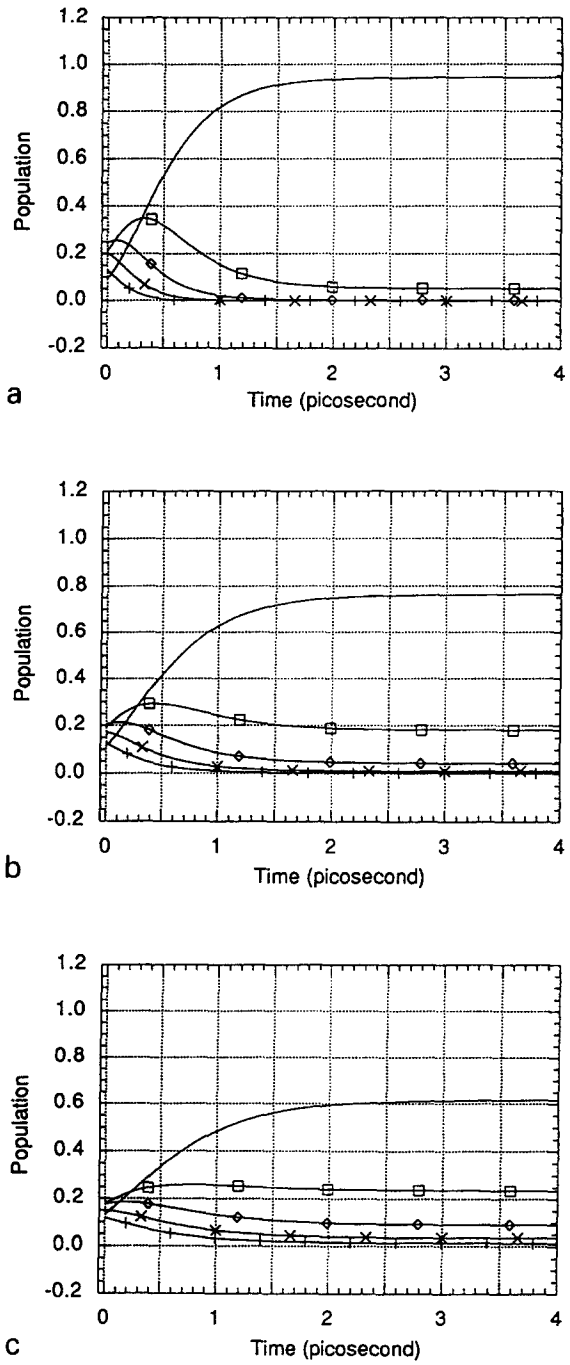

Fig. 3. Temperature dependence of temporal development of the vibrational populations. The populations in the states v = 0, 1, 2, 3 and 4 are calculated with Eq. (15). The labels and the parameters are the same as used in Fig. 1. The populations in the states $v = 2$ and 3 rapidly decay within 2 ps. Resulting in a turn-over feature in the time-development of the population in the state $v = 1$ within the first 0.5 ps time region. After 2.5 ps all the changes in time-development behavior of each state become a plateau and approach to the thermal equilibrated populations; $n_1/n_0 = 4.62 \cdot 10^{-2}$, $n_2/n_0 = 2.13 \cdot 10^{-3}$, $n_3/n_0 = 9.80 \cdot 10^{-5}$, $n_4/n_0 = 4.52 \cdot 10^{-6}$ (n_i being the population of the state i), which situation indicates that the thermal equilibration is achieved on a time-scale 2.5 ps.

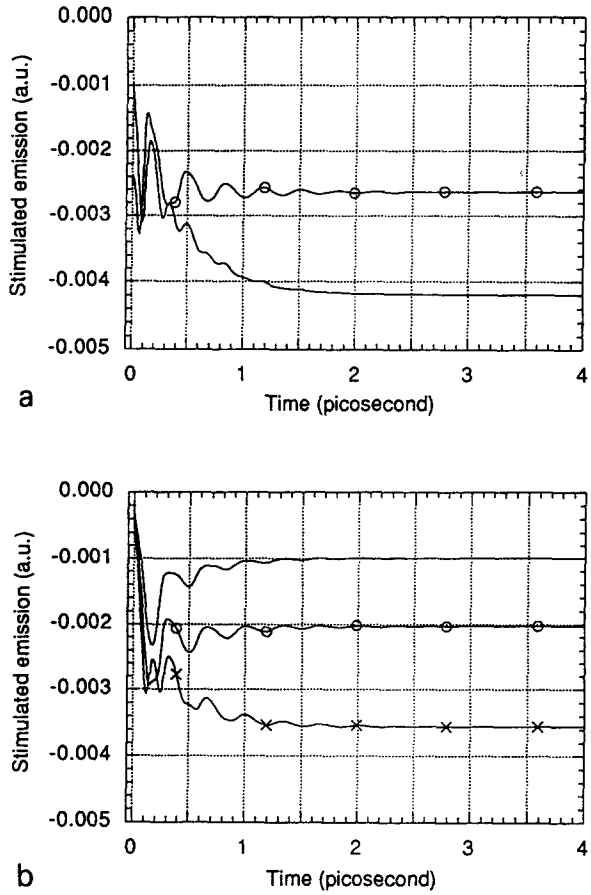

Fig. 4. Simulation of the time-resolved profiles of pump-probe stimulated emission at 50 K. The same parameters used in Fig. 2. are adopted for the calculation. (a) The pure solid line (a) The pure solid line and the one with ○ represent the time-resolved profile at 915 nm (10929 cm^{-1}) and 900 nm (11111 cm^{-1}), respectively: (b) the pure solid line, the ones with ○ and × depict the profiles at 960 nm (10417 cm^{-1}) and 930 nm (10753 cm^{-1}), respectively. The system still maintains the information of the coherent excitation in the first 1.0 ps time region so that quantum beats can be seen in this time region.

Now we shall investigate coupling constant dependence of time-resolved profiles at 10 K. Figs. 7 and 8 show simulation of time-resolved profiles with coupling constants of $S = 0.5$ and 1.0, respectively. The rest of the parameters are the same as used in Fig. 2. Fig. 7a clearly shows that, resulting from the fact that the peak position of the stimulated emission is located at near 900 nm [2], the phases of the quantum beats in the time-resolved profiles at 900 and 915 nm are in an out-of-phase relation. A similar relation can be seen between the quantum beat at 900 nm in Fig. 7a and the ones shown in Fig. 7b. Showing less change in intensity of the center of the amplitude, each quantum beat in Fig. 7 implies that the vibrational population transfer is not an important process for the pump-probe stimulated emission in the case of $S = 0.5$. This is mainly due to the fact that the optical transition from $u = 0$ to $v = 0$ is the most probable excitation in this case.

The situation changes in the case of $S = 1.0$. Fig. 8 indicates that the vibrational population transfer significantly affects the emission processes. However, the quantum beats remain longer compared with the case of $S = 2.5$.

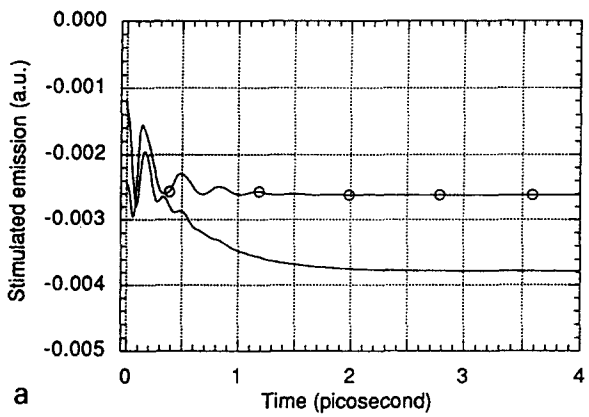

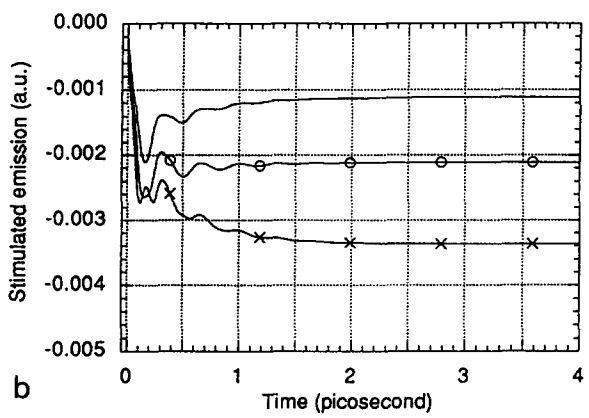

Fig. 5. Simulation of time-resolved profile of pump-probe stimulated emission at 100 K. The labels and the parameters are the same as used in Fig. 2. Rapid decreases in amplitude can be seen within the first 2.0 ps time region. The dephasing rate increases through the thermally activated vibrational transitions that are associated with the term with the Boltzmann factor in Eq. (21). Most part of the oscillatory features can be found in the first 1.0 ps time region.

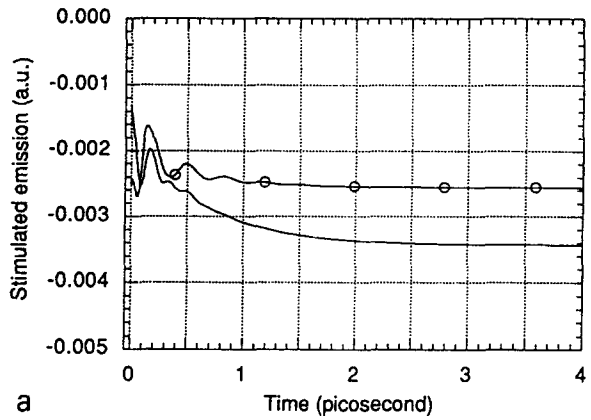

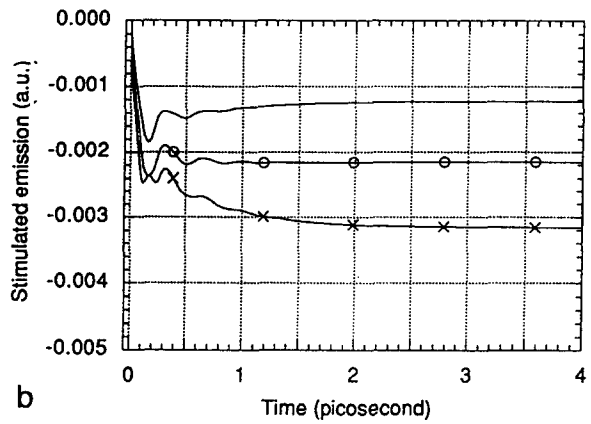

Fig. 6. Simulation of time-resolved profile of pump-probe stimulated emission at 150 K. The labels and the parameters are the same as used in Fig. 2. After 2 ps, the time profiles at 900, 915 and 930 nm decrease in intensity more rapidly compared with the profiles as shown in Figs. 4 and 5. At those probing frequencies the profiles reflect the population in the state $v = 0$. At the other frequencies the profiles gain intensity as the temperature increases. This is due mainly to the thermal equilibration of the vibrational states.

The optical transitions from the ground state to the higher vibrational levels, e.g., $v = 2$ or 3 are not favorable excitations in the case of $S = 1.0$. Our simulations and the quantum beats reported by Vos et al. clearly suggest that the minima of the ground state and electronically excited state potentials of the special pair of the D_{LL} mutant RC of *Rb. capsulatus* are rather strongly displaced along the intra-dimer coordinate.

In conclusion, on the basis of the perturbative density matrix method and the nonlinear susceptibility theory, we have derived an expression for the pump-probe stimulated emission profiles. Taking into account vibrational relaxation and thermally activated processes, we have investigated the effect of temperature on the time-resolved profiles of pump-probe stimulated emission. It becomes clear that, intensifying the dephasing processes, the vibrational transition processes result in the decrease of quantum beat amplitude as the temperature increases. We have applied our theory to analysis of the experimental results reported

by Vos et al. Our simulations agree qualitatively with their experimental results, although we have excluded a small frequency which appeared in the Fourier analysis of the their experimental data. We conclude that the rate constant of the vibrational relaxation of the vibrational mode of 100 cm^{-1} in the special pair is approximately 3.0 ps^{-1}. This is also consistent with a previous paper [40] and a relaxation time of 200 fs reported by Small's group whose analyses was based on hole-burning spectra of chemically altered RCs of *Rb. sphaeroides* and wild type RCs of *Rps. viridis* [45].

Finally, we also investigated the effects of temperature on pump-probe stimulated emission from a system consisting of two modes, that is, $\omega_l = 100$ cm^{-1} and $\omega_s = 30$ cm^{-1}, although we have not reported them in this paper. We found that the coherent excitation of the low-frequency mode at 10 K resulted in a pronounced slow oscillatory component in the time-resolved profile, modulating a rapid oscillatory component that was due to the coherent excitation of the high-frequency mode. At 50 and 150 K, on the other hand, we could not see such a slow oscillatory component since the thermal equilibration affect the low-frequency oscillation more rapidly. At 100 K, in particular, a fast oscillatory component quickly decreased in amplitude. The experimental data reported by Vos et al. [2], however, showed a slow oscillatory component at low temperature and it remained up to near room temperature. The mechanism of this particular feature of the slow oscillatory component should be explained in future studies.

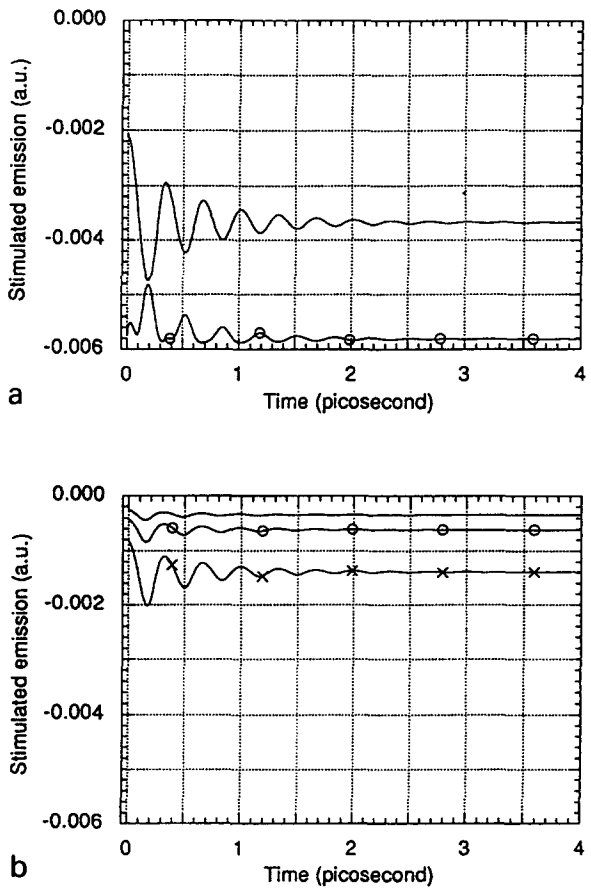

Fig. 7. Simulation of time-resolved profile of pump-probe stimulated emission at 10 K with $S = 0.5$. The rest of the parameters and the labels are the same as used in Fig. 4. (a) The phases of the quantum beats in the time-resolved profiles at 900 and 915 nm are in an out-of-phase relation. A similar relation can be seen between the quantum beat at 900 nm in the panel (a) and the ones shown in the panel (b). The vibrational population transfer is not an important process for the pump-probe stimulated emission in the case of S = 0.5 because the optical transition from $u = 0$ to $v = 0$ is the most probable excitation in this case.

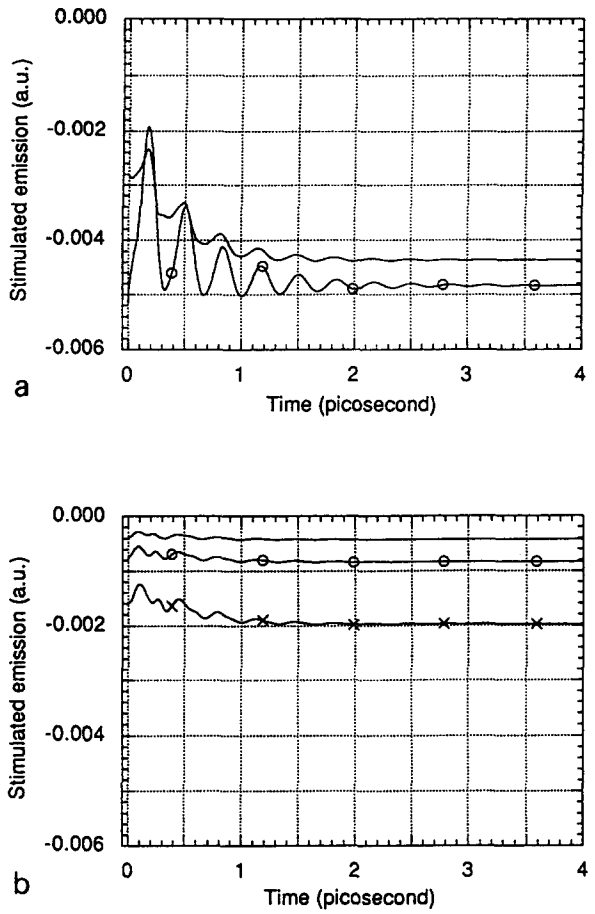

Fig. 8. Simulation of time-resolved profile of pump-probe stimulated emission at 10 K with $S = 1.0$. The rest of the parameters and the labels are the same as used in Fig. 4. The vibrational population transfer significantly affects the emission processes. The quantum beats remain longer compared with the case of $S = 2.5$. The optical transitions from the ground state to the higher vibrational levels, e.g., $v = 2$ or 3 are not favorable excitations in the case of $S = 1.0$.

Acknowledgements

This work was supported by Academia Sinica and the NSC of the Republic of China. The authors thank the referees for helpful comments and suggestions.

References

[1] Vos, M.H., Lambry, J.-C., Robles, S.-J., Youvan, D.C., Breton, J. and Martin, J.-L. (1991) Proc. Natl. Acad. Sci. USA 88, 8885–8889.
[2] Vos, M.H., Rappaport, F., Lambry, J.-C., Breton, J. and Martin, J.-L. (1993) Nature 363, 320–325.
[3] Peteanu, L.A., Schoenlein, R.W., Wang, Q., Mathies, R.A. and Shank, C.V. (1993) Proc. Natl. Acad. Sci. USA 90, 11762–11766.
[4] Martin, J.-L., Breton, J., Hoff, A.J., Migus, A. and Antonetti, A. (1986) Proc. Natl. Acad. Sci. USA 83, 957–961.
[5] Vos. M.H., Lambry, J.-C., Robles, S.J., Youvan, D.C., Breton, J. and Martin, J.-L. (1992), Proc. Natl. Acad. Sci. USA 89, 613–617.
[6] Chan, C.-K., DiMagno, T.J., Chen, L.X.-Q., Norris, J.R. and Fleming, G.R. (1991) Proc. Natl. Acad. Sci. USA 88, 11202–11206.
[7] Michel-Beyerle, M.E., Plato, M., Deisenhofer, J. (1989) Biophys. Acta 932, 52–70.
[8] Du, M., Rosenthal, S.J., Xie, X., DiMagno, T.J., Schmidt, M., Hanson, D.K., Schiffer, M., Norris, J.R. and Fleming, G.R. (1992) Proc. Natl. Acad. Sci. USA 89, 8517–8521.
[9] Holzapfel, W., Finkele, U., Kaiser, W., Oesterhelt, D., Sheer, H. Stilz, H.U. and Zinth, W. (1989) Chem. Phys. Lett., 160, 1–7.
[10] Hamm, P., Gray, K.A., Oesterhelt, D., Feick, R., Sheer, H. and Zinth, W. (1993) Biochim. Biophys. Acta 1142, 99–105.
[11] Kirmaier, C. and Holten, D. (1990) Proc. Natl. Acad. Sci. USA 87, 3552–3556.
[12] Bixon, M., Jortner, J. and Michel-Beyerle, M.E. (1991) Biochim. Biophys. Acta. 1056, 301–315.
[13] Holzapfel, W., Finkele, U., Kaiser, W., Oesterhelt, D., Sheer, H., Stilz, H.U. and Zinth, W. (1990) Proc. Natl. Acad. Sci. USA 87, 5168–5172.
[14] Lauterwasser, C., Finkele, U., Scheer, H. and Zinth, W. (1991) Chem. Phys. Lett. 183, 471–477.
[15] Dressler, K., Umlauf, E., Schmidt, S., Hamm, P. Zinth, W., Buchanan, S. and Michel, H. (1990) Chem. Phys. Lett. 183, 270–276.
[16] Schmidt, S., Arlt, T., Hamm, P. Lauterwasser, C., Finkele, U., Drews, G. and Zinth, W. (1993) Biochim. Biophys. Acta 1144, 385–390.
[17] Arlt, T., Schmidt, S., Kaiser, W., Lauterwasser, C., Meyer, M., Scheer, H. and Zinth, W. (1993) Proc. Natl. Acad. Sci. USA 90, 11753–11761.
[18] Martin, J.-L., Breton, J., Hoff, A.J., Migus, A. and Antonetti, A. (1986) Proc. Natl. Acad. Sci. USA 83, 957–961.
[19] Woodbury, N.W., Becher, M., Middendorf, D. and Parson, W.W. (1985) Biochemistry 24, 7516–7521.
[20] Friesner, R.A. and Won, Y. (1989) Biochim. Biophys. Acta 977, 99–122.
[21] Du, M., Rosenthal, S.J., Xie, X., DiMagno, T.J., Schmidt, M., Hanson, D.K., Schiffer, M., Norris, J.R. and Fleming, G.R. (1992) Proc. Natl. Acad. Sci. USA 89, 8517–8521.
[22] Chan, C.K., Chen, Lin, X.-Q., DiMagno, T.J., Hanson, D.K., Nance, S.L., Schiffer, M., Norris, J.R. and Fleming, G.R., (1991) Chem. Phys. Lett. 176, 366–372.
[23] Martin, J.-L. and Vos, M.H. (1992) Rev. Biophy. Biomolec. Struct. 21, 199–222.
[24] Fleming, G.R., Martin, J.L. and Breton, J. (1988) Science 333, 190–192.
[25] Wasielewski, M.R. (1988) Photochem. Photobiol. 47, 922–929.
[26] Maroti, P., Kirmaier, C., Wraight, C., Holten, D. and Pealstein, P.M. (1985) Biochim. Biophys. Acta, 810, 130–139.
[27] Bylina, E.J. and Youvan, D.C. (1988) Proc. Natl. Acad. Sci. USA 85, 7226–7230.
[28] Kirmaier, C., Holten, D., Bylina, E.J. and Youvan, D.C. (1988) Proc. Natl. Acad. Sci. USA 85, 7562–7566.
[29] Rees, D.C., Komiya, H., Yeates, T.O., Allen, J.P. and Feher, G. (1989) Ann. Rev. Biochem. 58, 607–633.
[30] Budil, D.E., Gast, P., Change, C.-H. and Norris, J.R. (1987) Ann. Rev. Phys. Chem. 38, 561–583.
[31] Deisenhofer, J. and Michel, M. (1989) Science 245, 1463–1473.
[32] Dutton, P.L., Kaufmann, K.J., Chance, B. and Rentzepis P.M. (1975) FEBS Lett. 60, 275–280.
[33] Kirmaier, C., Holten, D. and Parson, W.W. (1985) Biochemistry 24, 7516–7521.
[34] Wasielewski, M.R. and Tiede, D.M. (1986) FEBS Lett. 204, 368–372.
[35] Chekalin, S.V., Matveetz, Ya.A., Shkurapatov, Ya., Shuvalov, V.A. and Yartzev, A.P. (1987) FEBS Lett. 216, 245–248.
[36] Marcus, R.A. (1987) Chem. Phys. Lett. 133, 471–477.
[37] Lockhart, D.J., Goldstein, R.F. and Boxer, S.G. (1988) J. Chem. Phys. 90, 1048–1215; Boxer, S.G., Biophys, J. (1991) 59, 139a.
[38] Scherer, P.O.J. and Fischer, S.F. (1989) Chem. Phys. 133, 115–127.
[39] Lockhart, D.J., Kirmaier, C., Holten, D. and Boxer, S.G. (1990) J. Phys. Chem. 94, 6987–6995.
[40] Alden, R.G., Cheng, W.D. and Lin, S.H. (1992) Chem. Phys. Lett. 194, 318–326.
[41] Warshel, A. (1980) Proc. Natl. Acad. Sci. USA 77, 3105–3109.
[42] Johnson, S.G., Tang, D., Jankowiak, R., Hayes, J.M., Small, G.J. and Tiede, D.M. (1990) J. Phys. Chem. 94, 5849–5855.
[43] Small, G.J., Hayes, J.M. and Silbey, R.J. (1992) J. Phys. Chem. 96, 7499–7501.
[44] Middendorf, L.T., Mazzola, L.T., Gaul, D.F., Schenck, C.C. and Boxer, S.G. (1991), J. Phys. Chem. 95, 10142–10151.
[45] Lyle, P.A., Kolaczkowski, S.V. and Small, G.J. (1993) J. Phys. Chem. 97, 6924–6933; Reddy, N.R.S., Kolaczkowski, S.V. and Small, G.J. (1993) *ibid.*, 6934–6940.
[46] Reddy, N.R.S., Kolaczkowski, S.V. and Small, G.J. (1993) Science 260, 68–71.
[47] Marcus, R.A. (1956) J. Chem. Phys. 24, 966–978.
[48] Levich, V.G. (1966) J. Phys. Chem. 78, 249–371.
[49] Kestner, N.R., Logan, J. and Jortner, J. (1978) J. Phys. Chem. 78, 2148–2166.
[50] Hopfield, J.J. (1977) Biophys. J. 18, 311–321.
[51] Chu, Z.T., Lin, Y.Y. and Lin, S.H. (1987) J. Mol. Sci. 5, 127–138; Lin, S.H. (1989) J. Chem. Phys., 90, 7103–7113.
[52] Procyk, A.D. and Bocian, D.F. (1992) Annu. Rev. Phys. Chem. 43, 465–497.
[53] Palaniappan, V., Martin, P.C., Chynwat, V., Frank, H.A. and Bocian D.F. (1993) J. Am. Chem. Soc. 155, 12035–12049.
[54] Eyring, H., Lin, S.H. and Lin, S.M. (1980) Basic Chemical Kinetics, Wiley–Interscience, Chapter 7.
[55] Alden, R.G., Hayashi, M., Allen, J.P., Woodbury, N.W., Murchison, H. and Lin, S.H. (1993), Chem. Phys. Lett. 208, 350–358.
[56] Lin, S.H., Alden, R.G., Hayashi, M., Suzuki, S. and Murchison, H.A. (1993) J. Phys. Chem. 97, 12566–12573.
[57] Sugawara, M., Fujimura, Y., Yen, C.Y. and Lin, S.H. (1990) J. Photochem. Photobio. A54, 321–331.
[58] Lin, S.H., Alden, R.G., Tang, C.K., Fujimura, Y. and Sugawara, M. (1991) Mode Selective Chemistry (Jortner, J. et al., eds.), pp. 467–484, Kluwer, Dordrecht.
[59] Fain, B., Lin, S.H. and Hamer, N. (1989) J. Chem. Phys. 91, 4485–4494.
[60] Lin, S.H., Fain, B. and Hamer, N. (1990) Adv. Chem. Phys. 79, 133–267.
[61] Lin, S.H. and Villaeys, A.A. (1991) Density Matrix Method and Femtosecond Processes, World Scientific.
[62] Lin, S.H. (1974) J. Chem. Phys. 61, 3810–3820.